AGU100 ADVANCING EARTH AND SPACE SCIENCE

Geophysical Research Letters

RESEARCH LETTER
10.1029/2018GL079399

Key Points:
- Horizontal resolution strongly impacts exchange between shelf seas and the deep ocean
- Internal processes have a significant impact, as on-shelf transport increases within 20- to 150-m depth
- Increased off-shelf flux below 150-m depth has potential impacts for the shelf sea carbon pump

Correspondence to:
J. A. Graham,
jennifer.graham@cefas.co.uk

Citation:
Graham, J. A., Rosser, J. P., O'Dea, E., & Hewitt, H. T. (2018). Resolving shelf break exchange around the European northwest shelf. *Geophysical Research Letters*, *45*, 12,386–12,395. https://doi.org/10.1029/2018GL079399

Received 28 JUN 2018
Accepted 30 OCT 2018
Accepted article online 6 NOV 2018
Published online 20 NOV 2018

Resolving Shelf Break Exchange Around the European Northwest Shelf

Jennifer A. Graham[1,2], Jonathan P. Rosser[1], Enda O'Dea[1], and Helene T. Hewitt[1]

[1]Met Office, Exeter, UK, [2]Centre for Environment, Fisheries and Aquaculture Science, Lowestoft, UK

Abstract Shelf seas act as a significant sink of carbon within the global ocean. This occurs as carbon is exported beneath the permanent oceanic thermocline through the downwelling circulation across the shelf break. This downwelling circulation is quantified here using two regional ocean model configurations of the European northwest shelf, with differing resolution (7- and 1.5-km grid spacing). The dominant mechanisms and impact of model resolution are assessed along the length of the shelf break. The total downwelling circulation is stronger at higher resolution, due to an increased on-shelf transport at internal depths (20–150 m) and increased off-shelf transport at the base of the water column. At internal depths, these differences increase seasonally, influenced by stratification. Key processes in cross-shelf exchange only begin to be resolved at O(1 km), implying that global models currently used to assess the carbon cycles will be missing these processes.

Plain Language Summary Shallow seas over continental shelves have a large impact on the global environment, acting as a sink in the global carbon cycle. Despite their importance, shelf seas are not well represented in global climate simulations. Climate models struggle to reproduce exchange between the shelf seas and deep ocean, due to the combination of large and small-scale processes involved. Around the European northwest shelf, water typically flows onto the continental shelf (toward the coast) in the surface ocean and off-shelf (toward the deep ocean) at the bottom. This downwelling circulation allows carbon to be exported into the deep ocean, away from the atmosphere. The strength of the downwelling circulation is calculated here using two ocean models with different horizontal resolution (7- and 1.5-km grid spacings). These models represent different processes, dependent on their resolution. The higher-resolution model (1.5-km grid spacing) is found to have a stronger downwelling circulation, and these differences increase seasonally during the summer. This shows that small-scale processes, which are missing in lower resolution models, have a large impact on exchange between the shelf seas and deep ocean. These processes are missing in many global models used for long-term climate projections.

1. Introduction

Shelf seas have a disproportionately large impact on the global environment. Turbulence, mixing, and river runoff provide a large source of nutrients, fueling increased productivity (e.g., Muller-Karger et al., 2005). Shelf seas then act as a net carbon sink, as carbon drawn down from the atmosphere can be isolated from the surface and exported off shelf into the deep ocean (e.g., Bauer et al., 2013; Chen & Borges, 2009; Frankignoulle & Borges, 2001; Laruelle et al., 2014). Accurate simulation of exchange between the shelf seas and deep ocean is therefore not only important for understanding the local shelf environment but also critical for accurate representation of the global climate and carbon cycle.

Despite their importance, shelf seas are still not well represented in many climate models (e.g., Holt et al., 2017). Downwelling circulation occurs around the European northwest shelf (NWS), with net on-shelf transport in the upper layer and off-shelf transport at the base of the water column. Many mechanisms contribute to shelf break exchange. Previous studies have focused on a two-layer circulation, balanced between a wind-driven surface layer and bottom Ekman layer (e.g., Holt et al., 2009). Small-scale processes, such as eddies, fronts, and internal tides, are known to have a significant role but have not been resolved in coarser-resolution models (~10-km resolution; e.g., Huthnance, 1995; Huthnance et al., 2009).

As key processes in cross-shelf exchange only begin to be resolved at O(1 km), coarser-resolution regional models, as well as global models used to assess the carbon and water cycle, are likely missing key processes.

Higher-resolution models (<1-km grid spacing) are regularly used to study shelf break processes on local scales, for example, at the Celtic and Malin shelf edges (e.g., Aslam et al., 2017; Stashchuk & Vlasenko, 2017; Vlasenko et al., 2014). These models are valuable for process understanding but cannot be used to determine shelf-wide transport budgets. A new generation of regional models has been developed, with kilometer-scale resolution across the entire NWS domain (Graham et al., 2018; Guihou et al., 2018). In this study, downwelling across the NWS is assessed with two regional models of differing resolution. This demonstrates the potential impact of resolving small-scale processes, for shelf break exchange across the region.

2. Model Description and Simulations

This study uses two regional model configurations of Nucleus for European Modelling of the Ocean, at version 3.6 stable (Madec, 2016). These configurations have been developed through the U.K. Joint Weather and Climate Research Programme, for operational ocean forecasting as well as ongoing scientific research. The existing operational domain is known as AMM7 (Atlantic Margin Model, 7-km resolution), with previous versions validated in O'Dea et al. (2012, 2017). A new domain, with increased horizontal resolution, has recently been developed. AMM15 (1.5-km resolution) has been introduced and validated by Graham et al. (2018) and will become operational in November 2018. Aside from the horizontal grid, AMM15 and AMM7 share many features and parameterizations. Key differences and similarities are outlined here.

AMM15 bathymetry and coastline are derived from EMODnet (EMODnet Portal, September 2015 release). Increased resolution allows increased detail to be represented in the model's bathymetry. This can enable improved representation of small-scale processes, particularly along the shelf break (e.g., Aslam et al., 2017). AMM7 bathymetry is derived from the coarser North West Shelf Operational Oceanographic System (NOOS) data set.

Both models use the same z^*-σ coordinate system (Siddorn & Furner, 2013), with 51 vertical levels. Terrain-following coordinates are fitted to a smoothed envelope bathymetry, with the level of smoothing based on a specified r_{max} value (where $r = (h_i - h_{i+1})/(h_i + h_{i+1})$ and $h_{i,i+1}$ are adjacent bathymetry points). For AMM15, r_{max} was chosen to be 0.1, compared to 0.24 in AMM7. AMM15 has rougher bathymetry, resolving steeper gradients and canyons along the shelf break, so this lower value was chosen to ensure stability, without the need to smooth the input bathymetry.

With similar vertical resolution, vertical parameterization schemes remain similar in the two configurations. The generic length-scale scheme is used to calculate turbulent viscosities and diffusivities (Umlauf & Burchard, 2003). Dissipation under stable stratification is limited using the Galperin limit of 0.267 (Holt & Umlauf, 2008). Bottom friction is controlled through a log layer, with a minimum drag coefficient of 0.0025 for both AMM15 and AMM7.

Horizontal resolution in AMM15 is sufficient for resolving the internal Rossby radius on the shelf. Therefore, only minimal eddy viscosity is applied in the lateral diffusion scheme. For momentum and tracers, bi-Laplacian viscosities are applied on model levels using coefficients of 6×10^7 and 1×10^5 m^4/s, respectively. For AMM7, as the Rossby radius is not resolved, additional viscosity and eddy diffusivity are parameterized. Bi-Laplacian viscosity is applied on model levels for momentum, with a coefficient of 1×10^{10} m^4/s. Horizontal eddy diffusivity is applied for tracers, with a coefficient of 50 m^2/s. Further information surrounding the core model configurations can be found in Graham et al. (2018) and O'Dea et al. (2017).

For this study, a 2-year simulation was run using both configurations, for 2012–2013. In addition to these, monthly simulations were run for each January and July during 1994–2011. Each simulation was initialized from long hindcasts for each respective model (running for 1980s onward), with >8 years spin-up prior to January 1994. Initial conditions differ between the two models, dependent on biases within the spun-up state. However, both models have been forced with the same surface and Atlantic ocean boundaries, with the aim of minimizing such differences. Both models were run without data assimilation. Surface forcing was provided by the European Centre for Medium-Range Weather Forecasts (ECMWF) atmospheric reanalysis product, ERA-Interim (Dee et al., 2011). Boundary conditions for the Atlantic are provided by the Global Seasonal Forecast System (GLOSEA) version 5 (Jackson et al., 2016; MacLachlan et al., 2015). Baltic boundary forcing differs between the two models, given by a mean climatology in AMM7, compared with daily forcing in AMM15 (Graham et al., 2018). For both models, full-depth output is obtained at hourly intervals throughout

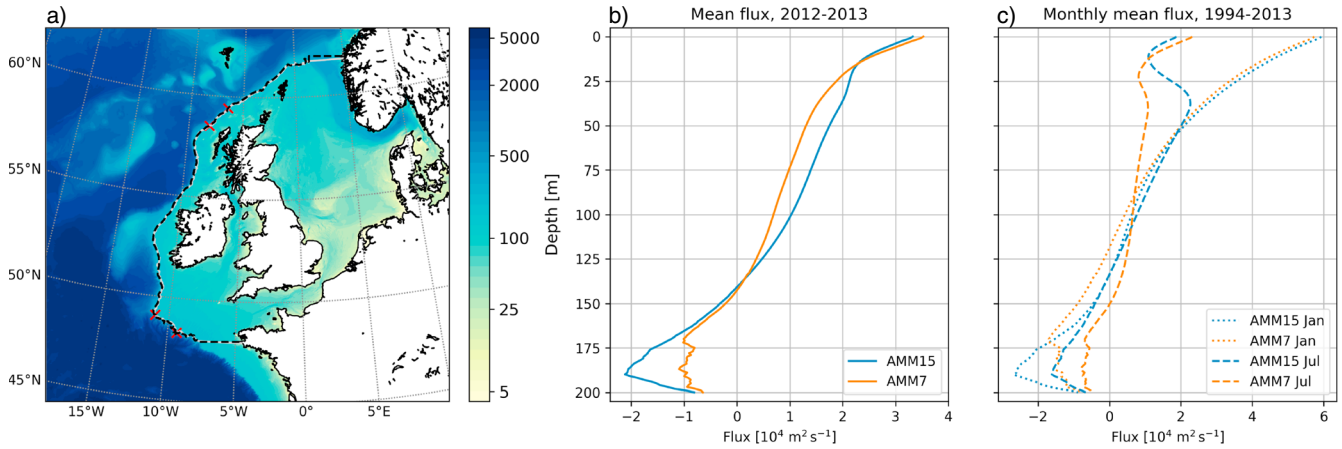

Figure 1. (a) Bathymetry across the AMM15 domain. Black dashed (solid gray) lines show location of shelf break for AMM15 (AMM7), defined as 200-m isobath, with gates at northern and southern limits. Red crosses indicate sections used for further analysis (section 3.2.2). (b, c) Shelf break flux per unit depth (m^2/s), for AMM15 (blue) and AMM7 (red). Positive values indicate flux in the on-shelf direction. Panels show (b) the mean flux over 2012–2013 and (c) the monthly mean fluxes over 1994–2013 for January (dotted) and July (dashed lines). Profiles shown are integrated along the shelf break shown in (a), excluding the gates. AMM = Atlantic Margin Model.

2012–2013, as well as additional monthly simulations, to resolve transport across the shelf break and seasonal variability during this period.

3. Results

3.1. Total Downwelling Circulation

Understanding the total downwelling circulation is critical for understanding cycling of water masses and nutrients across the NWS. Following previous studies, the shelf break is defined as the 200-m isobath (Figure 1a). At the northern and southern limits of the region, gates extend to the Norwegian and French coastlines. These close the region, allowing calculation of total fluxes onto and off the shelf. The location of the shelf break and gates differs slightly between the two models, due to differing model grids and bathymetry (Figure 1a; Graham et al., 2018); however, the same end points are used for total transport calculations, to enable model comparison. Total downwelling circulation is calculated as the net flux within the upper 150 m along the shelf break, compared to the net flux within the base of the water column (>150 m). This transport has been integrated along the shelf break and averaged over 2012–2013. The total downwelling circulation across the NWS is then 1.37 ± 0.24 Sv for AMM15 and 1.13 ± 0.15 SV for AMM7. AMM15 has a stronger downwelling circulation by 0.23 Sv, equivalent to a 21% increase from AMM7.

While the gates enable a closed transport to be calculated, the mechanisms responsible for transport along the Brittany coast and within the Norwegian Trench (NT) differ to those acting along the shelf break (primarily due to differing bathymetry). Therefore, to assess variability with depth, and mechanisms responsible for increased transport, fluxes have been summed along the shelf break (200-m isobath), excluding the gates. The resulting depth profiles (Figure 1b) show increased on-shelf flux in the upper portion of the water column and increased off-shelf flux in the base, consistent with an increased downwelling circulation.

In this study, the water column will be assessed within three depth sections. These will be referred to as the surface (<20 m), internal region (20–150 m), and base of the water column (>150 m). Transport within each section is dominated by different processes. These are analyzed in turn in section 3.2. Note that unless stated otherwise, any flux values that follow refer to totals calculated excluding the gates, for 2012–2013. Transport through the gates will be discussed in section 3.2.4.

3.2. Mechanisms for Shelf Break Exchange

3.2.1. Surface Fluxes

While the total downwelling circulation and depth profiles may differ, both models have a similar flux within the surface layer (<20 m; Figure 1b). The net on-shelf flux is 0.52 ± 0.08 Sv in AMM15 and 0.54 ± 0.08 Sv in AMM7. This suggests that both models have similar representation of surface fluxes along the shelf break, despite their different resolutions.

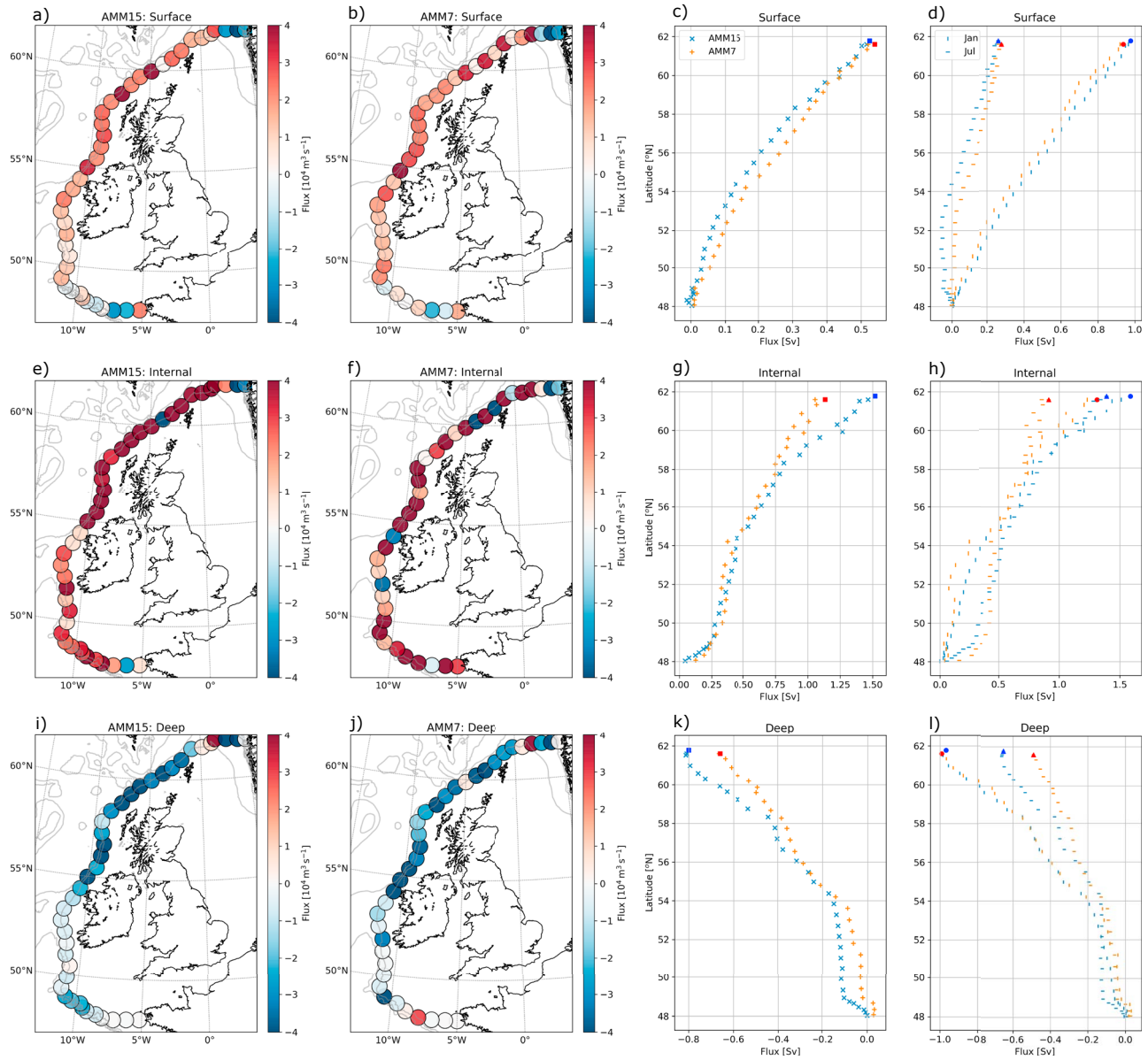

Figure 2. Time-mean volume fluxes integrated over depth. Panels show fluxes in (a–d) surface layer, <20 m; (e–h) internal depths, 20–150 m; and (i–l) base of the water column, >150 m. Each shaded marker represents the integrated flux (10^4 m^3/s) along ~60 km of the shelf break, for AMM15 (a, e, and i) and AMM7 (b, f, and j). Panels c and d, g and h, and k and l show the cumulative flux (Sv ≡ 10^6 m^3/s) with latitude (excluding the gates), for both AMM15 (blue) and AMM7 (red). Panels show (c, g, and k) mean fluxes over 2012–2013 and (d, h, and l) comparisons for January (vertical) and July (horizontal markers) over 1994–2013. Filled markers indicate total cumulative flux for the respective simulations at that depth. Note that the shelf break in AMM15 is longer than AMM7, so the number and position of markers is not consistent between panels.

The surface layer lies above the typical position of the pycnocline (Guihou et al., 2018). Fluxes here are then likely dominated by wind-forced Ekman transport. Prevailing southwesterly winds lead to a net on-shelf flux in the Ekman layer, due to the along-shelf component of wind stress. The average along-shelf component of surface stress in the ocean is approximately 0.012 N/m^2 in AMM15 and 0.016 N/m^2 in AMM7 (note that the shelf break is longer in AMM15, particularly along corrugated bathymetry around the Celtic Sea). This implies an Ekman transport of approximately 0.44 Sv for AMM15 and 0.45 Sv for AMM7. The majority of surface transport can then be attributed to Ekman transport.

The similarity in net surface fluxes is then not surprising since both models use the same surface forcing (ERA-Interim). Both models also show similar seasonal variability, consistent with stronger winds during winter (Figure 1c). Figures 2a–2d show the regional variability of surface fluxes along the shelf break. Stronger

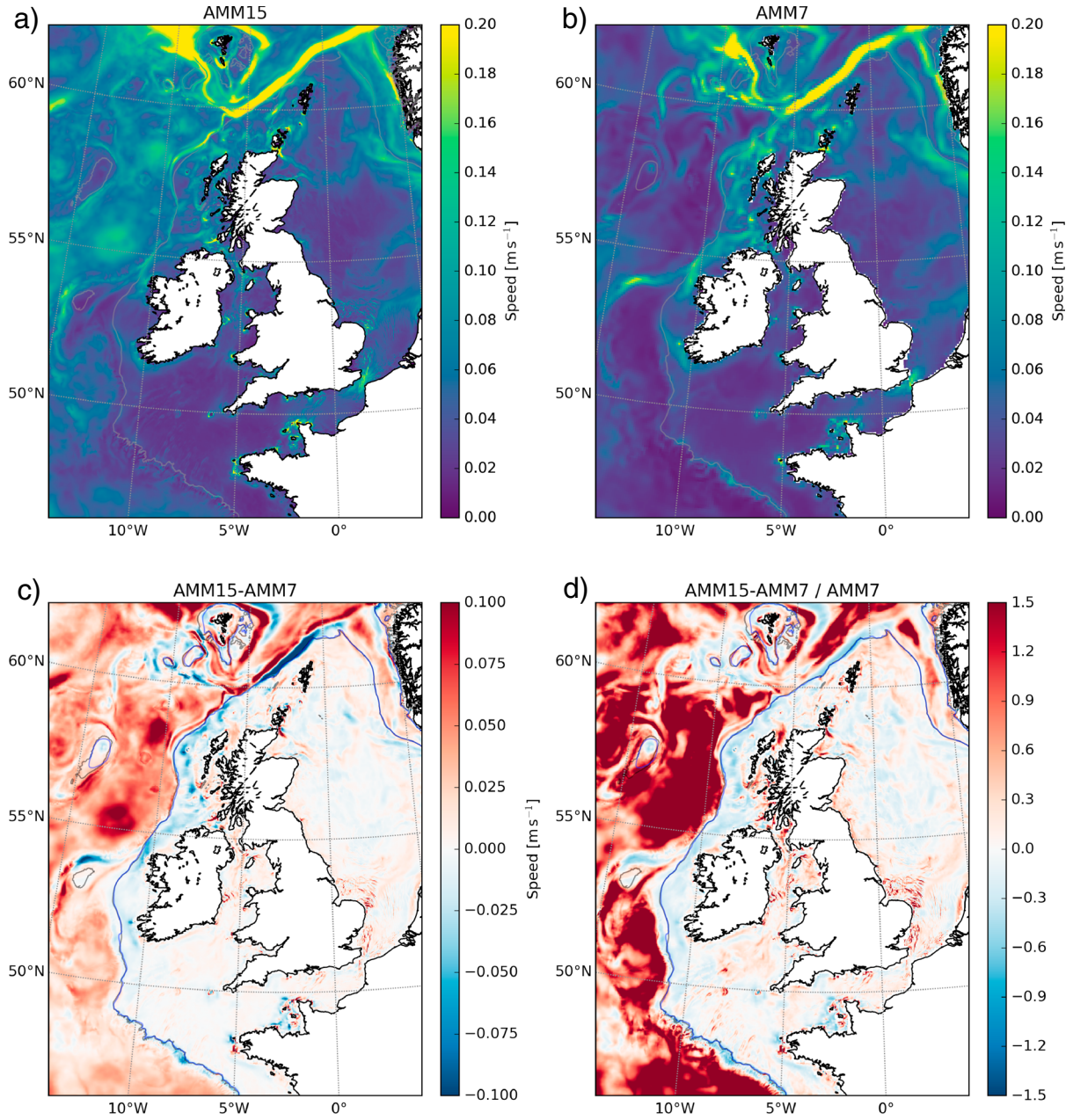

Figure 3. Mean barotropic current speed (m/s) for 2012–2013, for (a) AMM15, (b) AMM7, (c) AMM15 minus AMM7 anomaly, and (d) proportional anomaly, (AMM15 to AMM7)/AMM7. Contours are shown in panels (a, b) 200-m isobath for respective models (gray) and (c, d) 200-m isobath for AMM15 (gray) and AMM7 (blue).

on-shelf transport is found where the shelf break is aligned with prevailing southwesterly winds and increases during winter (Figure 2d).

Minor differences in surface stress likely occur due to the relative strength and direction of surface currents. Larger differences between the two models may occur on smaller spatial or temporal scales, as differences in surface currents become more significant. The total absolute flux in the surface layer shows an increase of ~20% from AMM7 to AMM15 during 2012–2013 (not shown). Therefore, while there is negligible difference in net flux, exchange of material across the shelf break does increase. Increased resolution of fine-scale currents is visible in AMM15 compared to AMM7 (Figures 3a and 3b). However, on the spatial and temporal scales considered here, wind forcing dominates the net surface transport.

3.2.2. Internal Fluxes

Internal fluxes are defined here as those within 20- to 150-m depth and are considered to be dominated by processes other than surface or basal Ekman forces. The net fluxes in this region are on shelf for both models but stronger in AMM15 (Figure 1b). The fluxes are 1.52 ± 0.16 Sv in AMM15, compared with 1.14 ± 0.08 Sv in AMM7, equivalent to a 31% increase. Both models have similar depth profiles in January, but differences between the two are amplified in July, predominantly at internal depths (Figure 1c). This internal transport forms a large majority of the total on-shelf flux.

While both models have similar representations of the large-scale circulation, resolution is likely to affect the representation of small-scale features. For example, the representation of bathymetry along the shelf break may affect the slope current, and increased resolution will allow AMM15 to resolve submesoscale processes (Guihou et al., 2018). All these factors may contribute to AMM15 having increased transport at internal depths.

Figures 2e–2h show the spatial variability of internal shelf break fluxes. Both models have similar mean fluxes and variability along the southern portion of the shelf break. However, AMM15 has much larger fluxes along the northern portion (>58°N; Figures 2g and 2h). Overall, there is an increased current speed in AMM15, compared with AMM7 (Figure 3). This is consistent with AMM15 resolving more submesoscale processes, such as eddies and fronts, throughout the deeper ocean. Along the shelf break, observations of the slope current have shown a speed of approximately 0.1–0.3 m/s, increasing toward to the north (Huthnance, 1995; Pingree et al., 1999; Souza et al., 2001). Both models reproduce this spatial variability, but the current is stronger in AMM15, coinciding with increased shelf break fluxes.

The slope current is believed to be driven by the combined effects of a meridional density gradient, wind forcing, and steep bathymetry (Huthnance, 1995; Marsh et al., 2017). Changes in current speed may then arise due to a combination of these factors. Despite the same boundary forcing, model biases and therefore density gradients may differ between the two configurations (Graham et al., 2018). However, the increased resolution of bathymetry in AMM15 is also likely to be a significant factor. This likely also accounts for shifts in position of the slope current, visible as dipoles in the anomaly field between ~ 58°N and 62°N (Figure 3c).

Both models show evidence of potential meanders in their slope currents, particularly along the northern half of the shelf break (Figures 3a and 3b). There is little evidence of increased persistence of such meanders in AMM15, compared with AMM7, with little increase in currents crossing the shelf break (Figures 3c and 3d). However, the increased speed in AMM15 suggests that any instabilities that do occur could result in increased transport.

Internal tides can be generated as the water column moves up and down across the continental slope with the barotropic tide. Displacement of the pycnocline generates oscillations that propagate away from the shelf break. These internal waves are nonlinear and can lead to significant fluxes onto the shelf (e.g.,Aslam et al., 2017; Vlasenko et al., 2014; Xing & Davies, 2001). Generation of internal tides is known to be stronger in particular areas, dependent on the continental slope (Huthnance, 1995). Around the NWS, increased energy has been observed around the Celtic Sea and off the west coast of Scotland (Malin Sea; e.g., Huthnance et al., 2009; Stashchuk & Vlasenko, 2017; Vlasenko et al., 2014). The M2 internal tide wavelength is ~10–20 km across the shelf; therefore, propagation cannot be resolved with a 7-km grid spacing Guihou et al. (2018). These processes begin to be resolved in AMM15, so may contribute to increased on-shelf fluxes at internal depths.

As internal tides are dependent on stratification, larger differences could be expected between the models during summer. This is consistent with the variability shown in Figure 1c, with increased on-shelf transport between ~20 and 100 m in AMM15 during July. Figure 4 shows the variability of flux with depth and time for two portions of the shelf break (Figure 1a). Sections were chosen for northwest Scotland (where the slope current speed has increased) and along the Celtic Sea (region of increased tidal energy). Temporal variability on submonthly time scales is similar between the two models, consistent with wind and tidally driven processes. Residual flow varies with the spring-neap cycle. However, differences become more apparent following the onset of stratification in May. For AMM15, there is an amplification of on-shelf transport along the pycnocline, at both locations. In addition to this, there is increased off-shelf transport in the lower portion of the water column.

Despite this difference, both models show similar seasonal variability in Figure 2h. It is worth noting here that increased off-shelf transport is not entirely confined to >150-m depth (Figures 1c and 4), thereby reducing the net on-shelf transport within internal depths. Further work is needed to quantify the impact of individ-

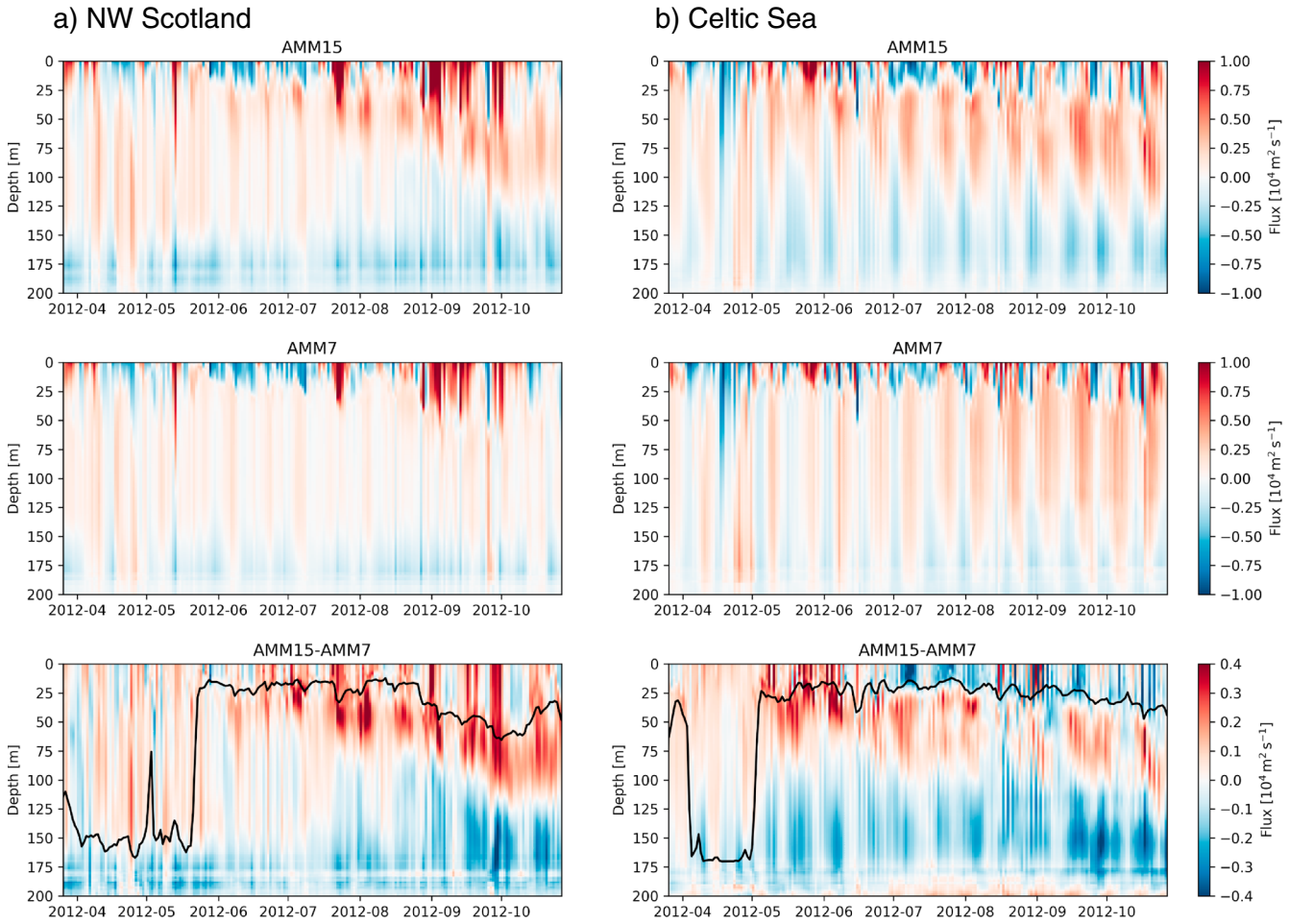

Figure 4. Flux per unit depth (m^2/s) for March–October 2012, integrated over sections (a) NW Scotland and (b) Celtic Sea, defined in Figure 1a. Panels show conditions in AMM15 (top row), AMM7 (middle row), and AMM15 minus AMM7 anomalies (bottom row). Positive values indicate on-shelf fluxes. Black lines shown in lower panels indicate the mixed layer depth in AMM15 (defined following de Boyer Montégut et al., 2004), averaged over the same section.

ual processes throughout the water column. Differences may become more significant when considering material transport in addition to volume fluxes. Figures 1c and 4 demonstrate that differences between the configurations are amplified under stratified conditions and focused around the pycnocline depth.

3.2.3. Basal Fluxes

The base of the water column (>150 m along the shelf break) is dominated by the influence of the seafloor. As the slope current flows northward, basal stress generates a bottom Ekman layer, producing a net off-shelf flux known as the Ekman drain. This off-shelf flux is found in both models (Figures 1b and 1c) but with significant differences in magnitude. The mean flux is -0.80 ± 0.13 Sv in AMM15 and -0.67 ± 0.08 Sv in AMM7. AMM15 has a stronger Ekman drain, ~20% greater than AMM7.

Various factors can influence the strength of the Ekman drain. First, Ekman transport is determined by basal stress and therefore the slope current. If we assume that basal stress is proportional to the velocity squared, then a 20% increase in Ekman transport equates to a velocity increase of ~10%. There is no consistent increase in the barotropic current along the shelf break (Figure 3). However, some regions show much larger changes, with increased current to the northwest of Scotland coinciding with increased off-shelf flux (Figures 2i–2l). Seasonal changes in the strength of the slope current (Marsh et al., 2017) likely account for an increased Ekman drain in winter (Figures 1c and 2l).

Another factor which likely affects the basal fluxes is bathymetry. Aside from affecting the volume of water available for off-shelf transport, the roughness of bathymetry may also impact basal stress. In the Celtic Sea, off-shelf fluxes increase in AMM15 (Figures 2i–2l; 48–49°N); however, the slope current appears weaker in this

region (Figure 3). Increased detail of bathymetry may be a key factor here, as AMM15 resolves steeper slopes and small-scale features such as canyons. These likely contribute to the increased Ekman drain along this region. The seasonality in basal fluxes differs between the north and south (Figure 2l), suggesting differences in either the slope current's seasonality or dominant mechanisms. Figure 4b shows that increased basal fluxes in the Celtic Sea during July may also be associated with internal tide processes.

3.2.4. Transport Through the Gates

Gates at the northern and southern ends of the shelf break are required to close transport within the region. In addition to the Ekman drain discussed in section 3.2.3, the net on-shelf flux above the shelf break (sections 3.2.1 and 3.2.2) is balanced by off-shelf flow in the NT. The NT contains southward flow on the western side and northward flow on the east. However, the net transport is off-shelf throughout the water column (Figure 2). Transport through the NT is greater in AMM15, with a total flux of -1.23 ± 0.12 Sv, compared to -1.09 ± 0.08 Sv for AMM7. Of this total, the flux below 150 m is -0.57 ± 0.10 Sv for AMM15 and -0.46 ± 0.07 Sv for AMM7.

Flow through the NT is influenced by the balance of conditions between the Atlantic and Baltic Sea. Baltic boundary forcing differs between the two models, so will likely contribute to the differences seen here. Quantifying the impact of Baltic boundary conditions in these regional models is an ongoing topic of research (Graham et al., 2018). However, while increased transport in the NT contributes to the total downwelling, it is not sufficient by itself to explain increased circulation across the NWS.

Through the southern gate, there is a negligible net transport in AMM15, compared with a net on-shelf flow in AMM7 (Figure 2), totaling -0.02 ± 0.02 Sv and 0.07 ± 0.01 Sv, respectively. This difference is likely due to changes in the residual tidal flow, influenced by changes in coastline, bathymetry, and tidal boundary forcing, between the models (Graham et al., 2018; Guihou et al., 2018).

4. Discussion and Conclusions

This study illustrates the potential impact of model resolution, and hence resolved processes, on exchange between shelf seas and the deep ocean. These two configurations give similar representations of the mean downwelling circulation, but it is significantly stronger at higher resolution, with an increase of ~20% in AMM15 compared to AMM7. Both models have similar wind-driven transport in the surface layer (<20-m depth). Increased on-shelf flow occurs predominantly at internal depths above the shelf break (20- to 150-m depth), where there is an average ~30% difference between the two configurations. Increased off-shelf flux occurs at the base of the water column along the shelf break and throughout depth within the NT. The depth profile of shelf break fluxes differs between the models. Anomalies vary seasonally with the onset of stratification, predominantly at internal depths. This suggests that model resolution is an important factor for understanding water mass and nutrient exchange across the region.

Internal processes make a significant contribution to the strength and variability of the downwelling circulation, contributing ~70% of the total on-shelf flux. Simple linear models that consider only surface and basal Ekman transports cannot accurately explain the behavior of this circulation. Understanding the processes responsible for this internal transport, and their representation in ocean models, is crucial for understanding variability of shelf break exchange.

Both models show similar regional variability, with the largest fluxes for both models (both on shelf and off shelf) found along the northern portion of the shelf break (>54°N). This spatial pattern is consistent with previous studies (Holt et al., 2009; Huthnance et al., 2009). Results here show that this is also where the largest differences occur between the two configurations, coinciding with a stronger slope current. Further analysis of the slope current, its variability, and its influence on shelf break fluxes would therefore be particularly worthwhile in this region. However, future model analysis should also investigate the impact of boundary conditions on the shelf break current. This may have a greater impact on the Celtic Sea, being closer to the southern boundary.

Variability of the downwelling circulation can have significant impacts on primary production as well as carbon export into the deep ocean (Holt et al., 2009). The mean off-shelf transport shown here would be equivalent to evacuating the bottom quarter of the water column across the shelf within 5 months for AMM15 (20% slower for AMM7). However, it has been shown that this circulation is nonuniform, over both space and time. With fluxes sensitive to seasonal stratification, this has implications for understanding shelf break exchange through future climate scenarios.

Overall, the increased downwelling in AMM15 suggests potential for increased draw down of carbon across the NWS at higher resolution. Work is ongoing to couple AMM15 with a biogeochemical model, to enable more thorough analysis of the impacts on productivity across the shelf (similar to Holt et al., 2016; Wakelin et al., 2012). For example, with the time scales and volume transport considered here, impacts of resolution were less significant for net surface fluxes. However, if nutrient content differs between opposing currents of similar strength, this could lead to larger differences between the two configurations, despite there being a negligible net volume flux.

Most global Earth system models use resolutions >7 km, lacking many processes acting at the shelf break (including tides; Holt et al., 2017). If such models are unable to parameterize shelf break processes effectively, then it is unreasonable to expect that they will accurately represent the downwelling circulation or its variability. This has significant implications for the interpretation and development of such models, which are used for long-term carbon cycle projections.

Acknowledgments
Simulations were carried out on the Cray HPC at the Met Office, UK. The data generated require a large tape storage facility (exceeding 100 TB). The data sets have been archived through the Met Office mass storage system and can be accessed through the STFC-CEDA platform JASMIN (Lawrence et al., 2013). Access to NEMO code and parameterizations used are outlined in Graham et al. (2018). This work was conducted through the U.K. Joint Marine Modelling Programme. Funding support is gratefully acknowledged from the Ministry of Defence, Public Weather Service, and Copernicus Marine Environment Monitoring Service.

References

Aslam, T., Hall, R. A., & Dye, S. R. (2017). Internal tides in a dendritic submarine canyon. *Progress in Oceanography*. https://doi.org/10.1016/j.pocean.2017.10.005

Bauer, J. E., Cai, W.-J., Raymond, P. A., Bianchi, T. S., Hopkinson, C. S., & Regnier, PierreA. G. (2013). The changing carbon cycle of the coastal ocean. *Nature*, *504*(7478), 61–70. Copyright - Copyright Nature Publishing Group Dec 5, 2013; Document feature - Diagrams; Graphs; Charts; ; Last updated - 2014-01-17; CODEN - NATUAS.

Chen, C.-T. A., & Borges, A. V. (2009). Reconciling opposing views on carbon cycling in the coastal ocean: Continental shelves as sinks and near-shore ecosystems as sources of atmospheric CO_2. *Deep Sea Research Part II*, *56*, 578–590.

de Boyer Montégut, C., Madec, G., Fischer, A. S., Lazar, A., & Iudicone, D. (2004). Mixed layer depth over the global ocean: An examination of profile data and a profile-based climatology. *Journal of Geophysical Research*, *109*, C12003. https://doi.org/10.1029/2004JC002378

Dee, D. P., Uppala, S. M., Simmons, A. J., Berrisford, P., Poli, P., Kobayashi, S., et al. (2011). The ERA-Interim reanalysis: Configuration and performance of the data assimilation system. *Quarterly Journal of the Royal Meteorological Society*, *137*(656), 553–597. https://doi.org/https://doi.org/10.1002/qj.828

Frankignoulle, M, & Borges, A. V. (2001). European continental shelf as a significant sink for atmospheric carbon dioxide. *Global Biogeochemical Cycles*, *15*(3), 569–576.

Graham, J. A., O'Dea, E., Holt, J., Polton, J., Hewitt, H. T., Furner, R., et al. (2018). AMM15: A new high-resolution NEMO configuration for operational simulation of the European north-west shelf. *Geoscientific Model Development*, *11*, 681–696.

Guihou, K., Polton, J., Harle, J., Wakelin, S., O'Dea, E., & Holt, J. (2018). Kilometric scale modelling of the North West European Shelf Seas: Exploring the spatial and temporal variability of internal tides. *Journal of Geophysical Research: Oceans*, *122*, 688–707. https://doi.org/10.1002/2017JC012960

Holt, J., Hyder, P., Ashworth, M., Harle, J., Hewitt, H. T., Liu, H., et al. (2017). Prospects for improving the representation of coastal and shelf seas in global ocean models. *Geoscientific Model Development*, *10*, 499–523.

Holt, J., Schrum, C., Cannaby, H., Daewel, U., Allen, I., Artioli, Y., et al. (2016). Potential impacts of climate change on the primary production of regional seas: A comparative analysis of five European seas. *Progress in Oceanography*, *140*, 91–115.

Holt, J., & Umlauf, L. (2008). Modelling the tidal mixing fronts and seasonal stratification of the Northwest European Continental shelf. *Continental Shelf Research*, *28*, 887–903.

Holt, J., Wakelin, S., & Huthnance, J. (2009). Down-welling circulation of the northwest European continental shelf: A driving mechanism for the continental shelf carbon pump. *Geophysical Research Letters*, *36*, L14602. https://doi.org/10.1029/2009GL038997

Huthnance, J. M. (1995). Circulation, exchange and water masses at the ocean margin: The role of physical processes at the shelf edge. *Progress in Oceanography*, *35*, 353–431.

Huthnance, J. M., Holt, J. T., & Wakelin, S. L. (2009). Deep ocean exchange with west-European shelf seas. *Ocean Science*, *5*, 621–634.

Jackson, L. C., Peterson, K. A., Roberts, C. D., & Wood, R. A. (2016). Recent slowing of Atlantic overturning circulation as a recovery from earlier strengthening. *Nature Geoscience*, *9*(7), 518–522.

Laruelle, G. G., Lauerwald, R., Pfeil, B., & Regnier, P. (2014). Regionalized global budget of the CO_2 exchange at the air-water interface in continental shelf seas. *Global Biogeochemical Cycles*, *28*, 1199–1214.

Lawrence, B. N., Bennett, V. L., Churchill, J., Juckes, M., Kershaw, P., Pascoe, S., et al. (2013). Storing and manipulating environmental big data with JASMIN. In *2013 Ieee International Conference on Big Data* (pp. 68–75). Silicon Valley, CA. https://doi.org/10.1109/BigData.2013.6691556

MacLachlan, C., Arribas, A., Peterson, K. A., Maidens, A., Fereday, D., Scaife, A. A., et al. (2015). Global seasonal forecast system version 5 (GLOSEA5): A high-resolution seasonal forecast system. *Quarterly Journal of the Royal Meteorological Society*, *141*, 1072–1084.

Madec, G. and the NEMO team (2016). NEMO reference manual 3_6_sctable: "NEMO ocean engine" note du pôle de modélisation, Institut Pierre-Simon Laplace (IPSL), France, no 27 ISSN no 1288-1619.

Marsh, R., Haigh, I. D., Cunningham, S. A., Inall, M. E., Porter, M., & Moat, B. I. (2017). Large-scale forcing of the European slope current and associated inflows to the North Sea. *Ocean Science*, *13*, 315–335.

Muller-Karger, F. E., Varela, R., Thunell, R., Luerssen, R., Hu, C., & Walsh, J. J. (2005). The importance of continental margins in the global carbon cycle. *Geophysical Research Letters*, *32*, L01602. https://doi.org/10.1029/2004GL021346

O'Dea, E. J., Arnold, A. K., Edwards, K. P., Furner, R., Hyder, P., Martin, M. J., et al. (2012). An operational ocean forecast system incorporating NEMO and SST data assimilation for the tidally driven European north-west shelf. *Journal of Operational Oceanography*, *5:1*, 3–17.

O'Dea, E., Furner, R., Wakelin, S., Siddorn, J., While, J., Sykes, P., et al. (2017). The CO5 configuration of the 7 km Atlantic Margin Model: Large-scale biases and sensitivity to forcing, physics options and vertical resolution. *Geoscientific Model Development*, *10*, 2947–2969.

Pingree, R. D., Sinha, B., & Griffiths, C. R. (1999). Seasonality of the European slope current (Goban Spur) and ocean margin exchange. *Continental Shelf Research*, *19*, 929–975.

Siddorn, J. R., & Furner, R. (2013). An analytical stretching function that combines the best attributes of geopotential and terrain-following vertical coordinates. *Ocean Modelling*, *66*, 1–13.

Souza, A. J., Simpson, J. H., Harikrishnan, M., & Malarkey, J. (2001). Flow structure and seasonality in the Hebridean slope current. *Oceanologica Acta*, *24*, 63–76.

Stashchuk, N., & Vlasenko, V. (2017). Bottom trapped internal waves over the Malin Sea continental slope. *Deep Sea Research Part I*, *119*, 68–80.

Umlauf, L., & Burchard, H. (2003). A generic length-scale equation for geophysical turbulence models. *Journal of Marine Research*, *61*(2), 235–265.

Vlasenko, V., Stashchuk, N., Inall, M. E., & Hopkins, J. E. (2014). Tidal energy conversion in a global hot spot: On the 3-D dynamics of baroclinic tides at the Celtic Sea shelf break. *Journal of Geophysical Research: Oceans*, *119*, 3249–3265. https://doi.org/10.1002/2013JC009708

Wakelin, S. L., Holt, J. T., Blackford, J. C., Allen, J. I., Butensch on, M., & Artioli, Y. (2012). Modeling the carbon fluxes of the northwest European continental shelf: Validation and budgets. *Journal of Geophysical Research*, *117*, C05020. https://doi.org/10.1029/2011JC007402

Xing, J., & Davies, A. M. (2001). Non-linear effects of internal tides on the generation of the tidal mean flow at the Hebrides shelf edge. *Geophysical Research Letters*, *28*(20), 3939–3942. https://doi.org/https://doi.org/10.1029/2001GL013308